Optics and Lasers in Engineering 68 (2015) 58–73

Contents lists available at ScienceDirect

Optics and Lasers in Engineering

journal homepage: www.elsevier.com/locate/optlaseng

Review

Review of RGB photoelasticity

A. Ajovalasit, G. Petrucci, M. Scafidi *

University of Palermo–Italy, DICGIM–Dipartimento di Ingegneria Chimica, Gestionale, Informatica, Meccanica, Viale delle scienze – edificio 8, 90128, Palermo, Italy

ARTICLE INFO

Article history:
Received 31 March 2014
Received in revised form
10 November 2014
Accepted 15 December 2014

Keywords:
RGB photoelasticity
Image acquisition and elaboration
Experimental mechanics

ABSTRACT

Automatic methods of photoelasticity have had a significant progress with the development of automatic acquisition and image processing methods. This article concerns RGB photoelasticity, which allows the determination of the photoelastic retardation using, usually, a single acquisition of the isochromatic fringes in white light by a colour camera. In particular, the article presents an overview of the main characteristics of RGB photoelasticity that is influence of the quarter-wave plate error, number of acquisitions, type of light source, determination of low and high fringe orders, methods for searching the retardation, scanning procedures, calibration on a material different from that under test, combined use of the RGB and phase shifting methods. A short section on the applications of RGB photoelasticity completes the article.

Contents

Abbreviations: ATPM, Automated Tint Plate Method; GFP, Gray Field Polariscope; LUT, Look-Up Table (calibration array); PSM, Phase Shifting Method; RGB, RGB Method; SCA, Spectral Content Analysis; TF-RGB, *Test fringes* RGB Method; TMCM, Tardy Manual Compensation Method

* Corresponding author.
E-mail addresses: a.ajovalasit@gmail.com (A. Ajovalasit), giovani.petrucci@unipa.it (G. Petrucci), michele.scafidi@unipa.it (M. Scafidi).

http://dx.doi.org/10.1016/j.optlaseng.2014.12.008
0143-8166/

1. Introduction

The development of automated methods of acquisition and processing of images has allowed the realization of several automated methods of photoelasticity based on the use of monochromatic or white light sources. In particular are cited the:

- Phase Shifting Methods (PSM) on monochromatic light and in white light;
- Fourier transform method;
- method known as Spectral Content Analysis (SCA);
- the method known as Gray Field Polariscope (GFP);
- tricolour Photoelasticity and other methods based on the use of white light;
- RGB photoelasticity.

Reviews on the above methods appear periodically in journals [1–5].

The Phase Shifting Method (PSM) in monochromatic light, introduced in 1986 by Hecker and Morche [6], generally requires at least four acquisitions. After the pioneering work of Hecker and Morche, a significant contribution was made by Patterson and Wang [7], who proposed a method based on the use of circularly polarized light incident on the model and six positions of the analyzer and its quarter wave plate. In the phase shifting method, the maps of the isocline parameter and of the relative retardation are obtained using the arctangent function applied to combinations of acquired light intensities. Because of the periodicity of the tangent function, the above maps are wrapped, it is therefore necessary to apply procedures of unwrapping. Various methods that minimize the influence of the error of quarter-wave plates on isochromatic and isoclines have been proposed [8,9]. For a survey on the phase shifting methods, the reader is referred to the literature [10].

The use of white light in the phase shifting methods has been considered for the determination of both the isoclinic parameter and the retardation. Thus the PSM in white light has been used by several researchers [11–13] in order to determine the isoclinic parameter, minimizing the interaction between isochromatics and isoclines and avoiding the use of light sources of several wavelengths [14]. Some authors [15] have shown that the spectral content of the light source influences the retardation and the isoclinic parameter, determined using a monochrome camera. The phase shifting method in white light was used for the determination of the retardation by Ramesh et al. [16,17].

An analysis of the phase shifting method in white light can be found in [18] with reference to the following aspects: spectral content of the light source, spectral response of the RGB filters of the camera, dispersion of birefringence and error of the quarter wave plates.

The Fourier transform method is based on the acquisition of isochromatics using carrier fringes obtained, for example, by a specimen subjected to bending or by means of a quartz wedge [19]. The retardation is determined using a single image. The benefit of using a single image is partly limited by the restriction due to the orientation of the principal stresses that need to be aligned (less than about 25°) in the model and in the carrier [20,21]. The combined effect of the error of quarter-wave plates and the misalignment of principal stresses between model and carrier is considered in [22].

The Spectral Content Analysis (SCA) [23–25] is based on the use of a spectrophotometer that determines, point by point, the spectral content of the light emerging from a circular polariscope illuminated in white light. The emerging intensity is compared with the theoretical intensity considered in an appropriate range of retardations. The unknown retardation is the one that minimizes the difference between experimental and theoretical values of the emerging light intensity. The SCA has also been proposed as a method in full field [26] by the use of a set of eight narrow band filters and a monochrome camera.

The Gray Field Polariscope (GFP) [27] is based on the use of circularly polarized monochromatic light incident on the model, the analysis is carried out using a rotating analyzer. In this way, the system acquires a large number of images using a camera, for what concerns the acquisition the GFP is therefore traceable to the phase shifting methods. The processing of the acquired images is used to determine the retardation and the parameter of the isoclines.

The so-called "tri-colour technique," based on the use of three wavelengths in plane polarized light, allows the determination of both isochromatics and isoclines [28,29]. The method uses a dark field plane polariscope illuminated by a source, which emits three narrowband wavelengths (Red at 619 nm, Green at 546 nm and Blue at 436 nm). Using a single acquisition and combining the light intensity detected at the three wavelengths, the retardation and the isoclinic parameter are determined.

Other methods in monochromatic light – The method using the variation of the load applied to the model (load stepping.) [30–33] allows to determine the retardation regardless of the isoclinic parameter, eliminating the ambiguities of the PSM. It is also not necessary to know the fringe order at one point.

Photoelasticity can also be used effectively to improve the discretization schemes in the finite element method [34,35]. Another field of application of digital photoelasticity regards the time average photoelasticity [36,37].

Other methods in white light – A method that is based on the acquisition of the isochromatic in dark and light field in a circular polariscope in white light by a colour CCD camera can be found in [38,39]. The subsequent subtraction of the above images allows the users to determine the points of zero intensity, which correspond to *apparent fringe orders*. Finally, using calibration curves that link the fringe order at a particular wavelength with apparent fringe orders, *actual fringe orders* are determined. A method based on the acquisition of four images using a plane polariscope, in dark field, and a three colour light source, has been proposed to eliminate the influence of quarter-wave plates errors [40]. Finally, Quiroga et al. in [41] have proposed the use of a regularization algorithm to demodulate the isochromatics acquired with a CCD camera using a fluorescent lamp as in discrete spectrum source.

This article concerns the RGB photoelasticity which is a full-field method for the determination of the photoelastic retardation

(isochromatic fringe order) using, usually, a single acquisition of white light isochromatics in a circular polariscope by a colour camera. The method was first introduced at the University of Palermo since 1990 [42] and subsequently published (1995) in an international context [43,44]. Initial further developments are due to Ramesh and Deshmukh [45] and Yoneyama and Takashi [46] who have proposed the use of elliptically polarized light to determine, in addition to the retardation, even the isoclinic parameter.

After the introduction of RGB photoelasticity, RGB applications in the fields of differential interferometry [47] and moiré-contouring [48–50] have been developed. The method called *Colourimetry-based retardation measurement* (CBRM) is similar to RGB photoelasticity. The model, illuminated in white light, is placed between two crossed polarizers. A spectrophotometer, however, is used in place of a colour camera [51].

General references to RGB photoelasticity are reported, in addition to the papers [42–45], in books [10,52–54] and in review papers [1–5].

In the following, after a brief account of the RGB method, the following aspects of RGB photoelasticity are considered:

- Influence of the quarter-wave plate errors;
- Number of acquisitions;
- Light source type and determination of fringe orders more than three;
- Determination of fringe orders less than 0.5;
- Search methods for the retardation;
- Scanning procedures;
- Calibration on a different material and effect of light intensity;
- Combined use of the RGB and phase shifting methods;
- Applications on birefringent coatings, glass residual stresses and others.

2. The RGB method in circularly polarized light

In the basic application of RGB photoelasticity, the model is placed in a circular polariscope, generally in dark field, and the isochromatic fringes are acquired in white light using a colour camera and a frame grabber. The camera decomposes the white light into the three primary colours red, green and blue by means of its three broad band filters and a frame grabber digitizes the three primary colours in three levels of intensity, which are usually denoted by the symbols *R*, *G* and *B*.

Due to the fact that the filters of the colour camera are broadband, the classical equation of the intensity emerging from a circular polariscope in dark field cannot be used. This equation has the following form

$$I = I_0 \sin^2 \pi\delta \tag{1}$$

in which, in the case of plane photoelasticity, the retardation δ is related to the difference of principal stresses $\sigma_1 - \sigma_2$ by the known relationship:

$$\delta = \frac{C_\lambda d}{\lambda}(\sigma_1 - \sigma_2) \tag{2}$$

d being the thickness of the photoelastic model and C_λ the photoelastic constant of the material at wavelength λ of the monochromatic light source used.

The relative retardation δ depends on the wavelength λ and on the dispersion of birefringence according to Eq. (2), which provides:

$$\delta = \delta_0 \frac{\lambda_0}{\lambda}\frac{C_\lambda}{C_0}, \tag{3}$$

where δ_0 and C_0 are, respectively, the relative retardation and the photoelastic constant at reference wavelength λ_0 and C_λ/C_0 represents the dispersion of the birefringence of the photoelastic material used [18,55,56].

The light intensity acquired by the colour camera, using a dark field circular polariscope with a white light source, can instead be expressed as [43]:

$$I_{wj} = \frac{1}{\lambda_{2j} - \lambda_{1j}} \int_{\lambda_{1j}}^{\lambda_{2j}} F_j(\lambda) I_0(\lambda) \sin^2(\pi\delta)\left(1 - \cos^2 2\alpha \sin^2 \varepsilon\right) d\lambda, \quad (j = R, G, B) \tag{4}$$

where $I_0(\lambda)$ is the intensity of the light source, F_j $(j = r, g, b)$ denotes the spectral response of the three filters of the camera, λ_{1j}, λ_{2j} are the minimum and maximum wavelengths relative to the three aforesaid filters, α indicates the orientation of the maximum principal stress, ε is the error of the retardation of quarter-wave plates and the subscript w indicates that the acquisition is carried out in white light.

The determination of the relative retardation δ by means of Eq. (4) is not easy so that a procedure based on a database search approach has been developed [42,43]. It consists of two phases, the *calibration*, in which the data base (herein called LUT: Look-Up Table) is created, and the *search of the retardation*, by using the data in the LUT.

2.1. Calibration and acquisition

In the calibration procedure, the levels *R*, *G* and *B* (Fig. 1) along the cross section of a specimen subjected to bending (Fig. 2) are acquired and stored in a database, the LUT, similar to the table of the colours used in the method of birefringent coatings.

Due to the fact that the retardation increases linearly along the calibration section, each triplet of the acquired RGB values can be easily associated to a value of the relative retardation δ_0, corresponding to a given reference wavelength λ_0. In particular, if δ_{0N} is the maximum retardation of the calibration table, N is the index corresponding to δ_{0N} and the first point acquired belong to the fringe of zero order, the relation between the index i of an element of the LUT and the retardation is

$$\delta_{0i} = \delta_{0N}\frac{i}{N}; \quad 0 \le i \le N \tag{5}$$

In order to obtain a good resolution in the evaluation of the retardation, the calibration should be carried out in such a way to obtain a large number of RGB triplets of the LUT (N»100). In order to maximize the differences among the colours in different ranges of the retardation it is important to maximize the modulation of the RGB signals acquired.

The *R*, *G* and *B* values stored in the LUT and that values acquired in the model to be analysed are influenced by the following factors:

- characteristics of the hardware: spectral properties, intensity and uniformity of the light source, spectral response of the filters of the camera, spatial and intensity resolution of the acquisition system;
- regulations of the hardware: aperture of the lens of the camera, white balance adjustment of the acquisition system;
- chromatic properties of the photoelastic material;
- gradient of the stress in the points of the model (in the case of calibration, it depends on the shape and loading system of the calibration specimen).

The light source that allows to obtain the greater modulation of the RGB signals is a tricolour source, that is, a source whose spectrum is composed of only three wavelengths [57,58]; a very

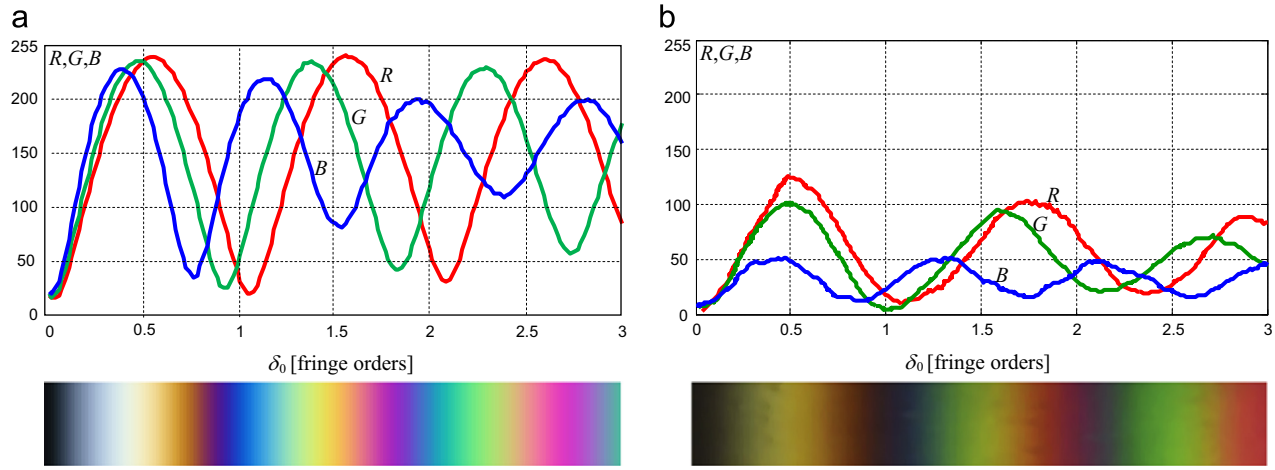

Fig. 1. Experimental RGB signals acquired from the isochromatic fringes of a bending specimen using a 8 bit digital system: a) obtained by the procedure recommended in this article; b) taken from literature.

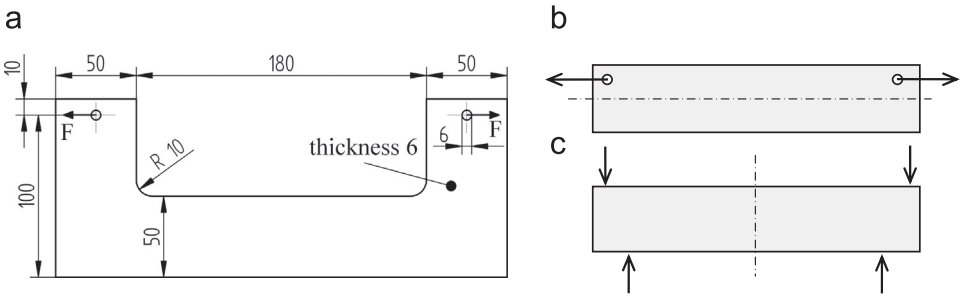

Fig. 2. Calibration specimens: a) the one proposed in the first paper on RGB photoelasticity (dimensions in mm); b) eccentrically loaded tensile specimen, c) four points bending specimen.

good modulation can be also obtained using commercially available fluorescent lamps with a discrete emission spectrum [41,59,60]. This aspect is detailed in Section 5.2.

Digital imaging systems with adequate spatial resolution (at least 640×400 pixels) and intensity resolution (at least 256 levels) are today widely available.

The aperture of the lens of the camera should be adjusted to fully exploit the intensity resolution of the digitizer, acquiring the light intensity levels near to the maximum intensity level of the digitizer.

The white balance of the image should be adjusted by the acquisition system (camera or digitizer) in such a way that the maximum values of the *R*, *G* and *B* signals assume similar values. This last aspect is particularly important when incandescent light source is used due to the fact that the blue signal is generally much lower than the red and green ones.

The number of elements of the LUT can be increased by properly adjusting the magnification of the optical system and by using suitably shaped calibration specimens, such as those of Fig. 2a and b. In particular these specimens allow to obtain a greater resolution with respect to four points bending specimens (Fig. 2c) due to the shifting of the neutral axis with respect to the centre of the specimen.

The shape and the dimensions of the specimen of Fig. 2a have been chosen in order to obtain ease of construction, ease of loading application, extended area for the determination of the LUT and higher value of the maximum fringe order during calibration. In any case, in the application of the load, care should be taken in order to avoid the presence of torsions in the specimen. The eccentrically loaded tensile specimen (Fig. 2b) [61] make it possible to obtain a greater shifting of the neutral axis with respect to the centre of the specimen, but requires the application of greater forces that increase the risk to introduce torsion and can hardly be used with fringe orders higher than three. The four points bending specimen (Fig. 2c) has the only advantage of a greater ease of construction.

Digital filtering and numerical procedures are also used to enhance the quality of the LUT. The number of triplets in the LUT can be increased using numerical techniques of interpolation [59,61,62]. In order to minimize the effect of electronic noise and non-uniformities of the light field in determination of the LUT, digital filtering techniques, such as median filtering, are also applied [61]. Nevertheless, considering the fact that the fringes in the calibration specimen are parallel, the simplest and efficient filtering method consists in determining each *R*, *G* and *B* level as the median of a great number of levels acquired along a line parallel to the fringes (50 at least).

In certain cases, it is appropriate to use the self-calibration procedure that does not require a calibration specimen [63]. This procedure is outlined in Section 7.2.1.

In Fig. 1 two examples of RGB signals acquired from a calibration specimen [60,64] are shown. The RGB signals in Fig. 1a has been acquired using a fluorescent light source and applying the procedure recommended in this article. The RGB signals of Fig. 1b has been acquired using incandescent light, the specimen shown in Fig. 2b, applying a two dimensional median filter; it appears that the white balance adjustment and the adjustment of the aperture of the lens of the camera to fully exploit the intensity resolution of the digitizer have not been carried out.

2.2. Search of the retardation

In the phase of search of the retardation, the *R*, *G* and *B* levels in the points of the photoelastic model where the retardation has to

be determined are acquired and compared with the R_i, G_i and B_i triplets stored in the LUT. The unknown retardation is the one corresponding to the values R_i, G_i and B_i that minimize an error function defined as:

$$e_i = \sqrt{(R-R_i)^2+(G-G_i)^2+(B-B_i)^2}. \quad (6)$$

To this end, in each pixel: (I) the error function given by (6) is calculated; (II) the index i that minimizes the above error function is determined; (III) the retardation in the point of interest is calculated using the relation (5); (IV) possible discontinuities are subsequently eliminated by a proper procedure (see Section 5.4).

In a general case the following equation can be used in place of Eq. (2) [65]

$$\delta_{0i} = (\delta_{0N}-\delta_{00})\frac{i}{N}+\delta_{00}; \quad 0 \le i \le N \quad (7)$$

where δ_{00} is the minimum retardation of the calibration table corresponding to the index of the first element $i=0$. Usually the analysis starts from the fringe of order 0 and Eq. (7) reduces to Eq. (5).

As it is detailed in Section 5.2, the maximum retardation that can be determined is about three orders fringe when using incandescent lamps and about twelve fringe orders when using fluorescent lamps. The experimental results show that the influence of the gradient of the fringes is negligible for gradients not exceeding 0.1 orders/pixel.

3. The RGB method in elliptically polarized light

A variation of the RGB method, which allows the determination of both the retardation and the isoclinic parameter from a single image in white light, has been proposed by Yoneyama and Takashi [46]. Instead of the traditional method, this one employs elliptically polarized light; in this case, the light intensity emerging from the three filters of the RGB camera can be expressed by the following approximate relationship:

$$I_i = \frac{9+\cos 2\varepsilon_i+5\cos 4\alpha+\cos 2\varepsilon_i\cos 4\alpha+4\sqrt{3}\sin\varepsilon_i\sin 4\alpha}{16}\frac{1}{\lambda_{i2}-\lambda_{i1}}\int_{\lambda_{i1}}^{\lambda_{i2}} F_i(\lambda)I_0(\lambda)\sin^2\left[\frac{\pi\Delta}{\lambda}\frac{C(\lambda)}{C_0}\right]d\lambda$$

$$(i = R, G, B) \quad (8)$$

where ε_i indicates the error of the quarter wave plate corresponding to the central wavelength of each filter of the camera and Δ indicates the absolute retardation.

The retardation is obtained by the procedure described in Section 2.2 based on the use, instead of the values R, G and B, of normalized values, the so-called *chromaticity coordinates* r, g and b given by:

$$r = \frac{R}{(R+G+B)},$$

$$g = \frac{G}{(R+G+B)},$$

$$b = \frac{B}{(R+G+B)} \quad (9\text{–}11)$$

From the retardation thus obtained, the determination of the isoclinic parameter is performed using the Eq. (8). Applications of the above technique concern the determination of stresses during a rolling contact [66] and the visco-elastic fracture [67].

4. Effect of the quarter wave plates error

Generally the circular polariscope uses chromatic quarter wave plates, corrected for the reference wavelength, usually monochromatic yellow (589 nm) or green (546 nm) lights. At different wavelengths, an error is introduced, whose effect on the determination of the retardation is considered in references [44,68].

For given retardation, if the values of the parameter α in the calibration specimen and in the points of the model (where it is necessary to determine the retardation) are different, then, according to Eq. (4), the values of R, G and B stored in the LUT are not equal to those measured on the model. Consequently, the retardation δ assumes an incorrect value called δ'. Eq. (4) in fact shows that the effect of the error the quarter wave plates depends on the isoclinic parameter α: this effect is null for $\alpha=45^\circ$ and is maximum for $\alpha=0^\circ$. A procedure for reducing this source of error is based on the calibration with the isoclinic parameter α set to the intermediate value of 22.5°. The error due to the quarter-wave plates can be avoided by using plane polarized light [11,69], in this case, however, four acquisitions are required.

4.1. Experimental results concerning the effect of the quarter-wave plate errors

The experimental tests [44] were performed in white light by using a polariscope with the quarter-wave plates of the polarizer and the analyzer, corrected for yellow light ($\lambda_0=589$ nm), with the axes crossed. A photoelastic specimen, subject to bending (Fig. 2) has been used both in the calibration phase and in the measurement phase. The levels R, G and B were measured along a cross section of the above specimen in light field and in dark field and for different values of the isoclinic parameter α. Fig. 3 shows the evolution of signal B for $\alpha=0^\circ$ and $\alpha=45^\circ$, in dark-field (Fig. 3a) and in light field (Fig. 3b). For $\alpha=0^\circ$ a decrease in the maximum intensity in dark-field and an increase of the minimum intensity in light field is observed.

The experimental results show that, using quarter wave plates corrected for monochromatic light yellow (589 nm) or green (546 nm), the maximum error of the retardation is respectively 0.05 and 0.03 fringe orders.

5. Characteristics of RGB photoelasticity

5.1. Number of acquisitions

Table 1 summarizes the number of acquisitions used in different versions of the RGB method. In the classic method (row 1), only one acquisition in the dark-field circular polariscope is performed. In addition, the method in elliptically polarized light requires a single acquisition [46]. In the second method (row 2), two acquisitions are made using the circular polariscope in light and dark field; in this case the differences of the R, G and B levels in light and dark field are used for the determination of the retardation. In the third method (row 3), the dark field plane polariscope is used to determine the isoclines with the phase shifting method in white light, the same four images provide the isochromatic fringes thus eliminating the error due to the quarter-wave plates. In the fourth method (row 4), the RGB and the phase shifting methods are used together as described in the Sections 5.2 and 6.

The first method is the simplest because it requires a single acquisition. It can then be used in the case of stress fields varying in time. The other methods lose this characteristic of simplicity. However, they allow the elimination of some spurious effects, also determine the isoclinic parameter (3rd method) and increase the maximum fringe order detectable (4th method).

5.2. Source type and determination of fringe orders over three

The light source initially proposed [43,45] and currently widely used is the common incandescent lamp which has a continuous

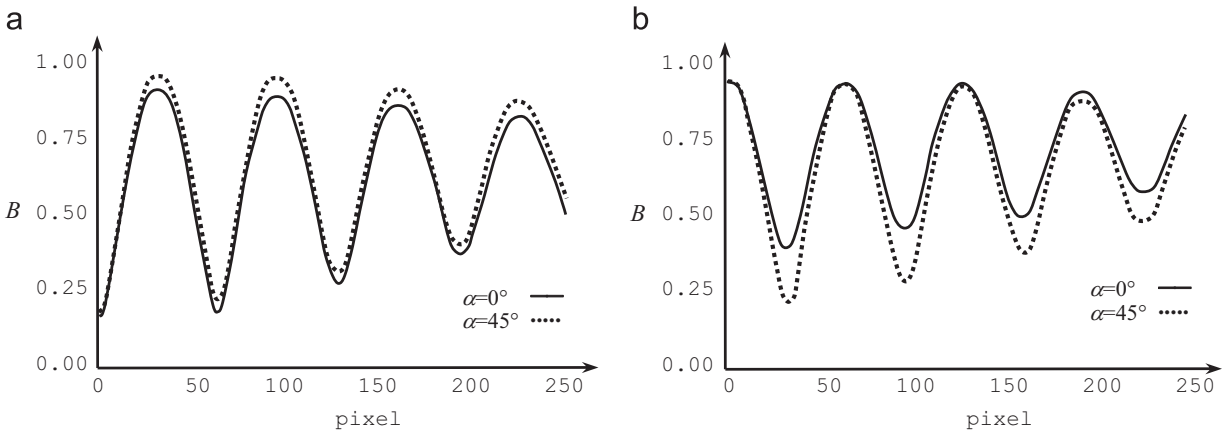

Fig. 3. Blue level (B) along the cross section of the calibration specimen for $\alpha=0^\circ$ and $\alpha=45^\circ$ in dark field (a) and in light-field (b).

emission spectrum of the type shown in Fig. 4a. The continuous emission spectrum is a major cause of the limitation of the detectable maximum fringe order. Therefore, subsequently, some authors have tried to raise the maximum fringe order detectable using light sources or filters with three narrow bands of wavelengths, as indicated below:

- use of a light source with three colours (narrow band) [57];
- use of a white light source and three narrow band filters (R, G and B) [58];
- use of fluorescent lamps with a discrete emission spectrum, [41,59], with such lamps the possibility of determining 20 fringe orders [59] or at least 12 fringe orders [60] is cited;
- use of a scanner with the ability to determine fringe orders up to five [71].

Again, in order to increase the maximum fringe order, some authors have used jointly the RGB method and the phase shifting one [70,72]. The measurable retardation is increased to about 5–6 fringe orders, with the drawback that 4/6 acquisitions are needed. Further details are provided in the dedicated Section 6.

In the following, the attention is focused on the comparison between two types of light sources: an incandescent lamp with a continuous spectrum (Fig. 4a) and a discrete spectrum fluorescent lamp (common energy-saving lamps), such as the Philips type Master LP 827 whose spectrum is shown in Fig. 4b. Fig. 5 shows a comparison between the experimental isochromatics in a beam subjected to bending, observed in the dark field circular polariscope, obtained using the two types of light sources. In particular, the following images are shown:

1. the isochromatic fringes in monochromatic yellow light ($\lambda_0=589$ nm);
2. the isochromatic fringes in white light;
3. the maps of the R, G and B levels related to the isochromatic fringes in white light.

Fig. 5 clearly shows that the visibility of the isochromatic fringes in white light remains high even for high fringe orders, when the fluorescent lamp is used.

This statement is confirmed by Fig. 6, which shows the RGB signals detected along the central cross section of the beam of Fig. 2, as a function of the retardation δ_0 at the reference wavelength $\lambda_0=589$ nm. Each R, G and B value in the figure has been determined as the median of the values acquired along a line parallel to the fringes, as previously suggested.

Table 1
Number of acquisitions used in several variants of RGB photoelasticity.

N°	Number of acquisitions	Polariscope	References
1	1	Circular in dark field	[43,45]
2	2	Circular in dark and light field	[45]
3	4	Plane in dark field	[11]
4	≥ 4	*Semicircular*	[70]

Fig. 6a shows that the modulation of the RGB signals acquired using the incandescent lamp, decreases rapidly with the increasing of fringe order, starting from $\delta \approx 2$. Consequently, RGB photoelasticity can be applied up to 3–4 fringe orders when an incandescent lamp is used. Fig. 6b shows that the modulation of the signals acquired using the fluorescent lamp decreases slowly with increasing fringe order and remains adequate at least up to 12 orders. The modulation is higher than that of the incandescent lamp also in the field $2 \leq \delta \leq 3$.

The use of fluorescent lamps with discrete emission spectrum is the most simple and cost effective way to increase the maximum retardation from three orders of fringe at least 12 orders that are more than enough in the usual investigations photoelasticity. Fluorescent lamps should be preferred in any case, due to the better modulation of the RGB signals in the field $2 \leq \delta \leq 3$.

Recently [54] the use of RGB LED has been proposed as a source of white light, with discrete spectrum, to be used in RGB photoelasticity, while the use of LED in monochromatic photoelasticity, has been documented since 1997 [73].

The maximum fringe order detectable by the RGB photoelasticity, however, depends in general on:

- the modulation of the signals R, G and B, mainly linked to the light source and the adjustments of the acquiring system (Figs. 5 and 6);
- the presence of similar colours and the procedure of search of the retardation;
- the gradient of the fringes, depending on the gradient of the stress field and on the characteristics of the acquiring system: resolution and magnification capability.

5.3. Determination of retardations less than 0.5 fringe orders

In the field of low levels of retardation ($0 \leq \delta \leq 0.5$ fringe orders) the isochromatic fringes appear in gray levels (Fig. 5) so that the R, G and B levels for each value of δ assume similar values (Fig. 6). In this case, high errors in the evaluation of the retardation

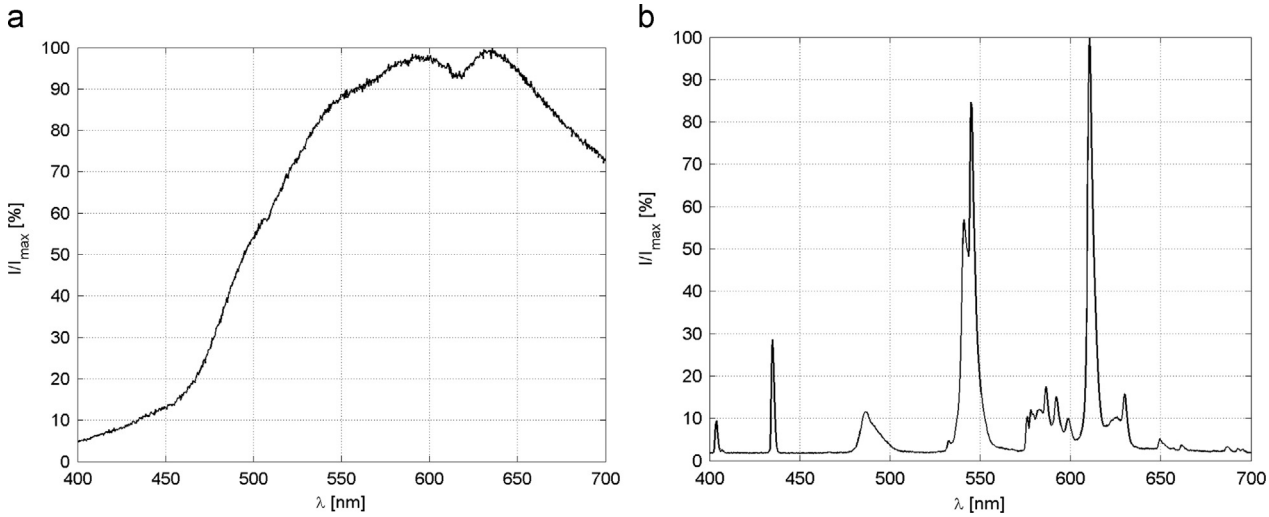

Fig. 4. Emission spectra of the light sources considered in this article: (a) continuous (common incandescent lamp), (b) discrete (fluorescent lamp).

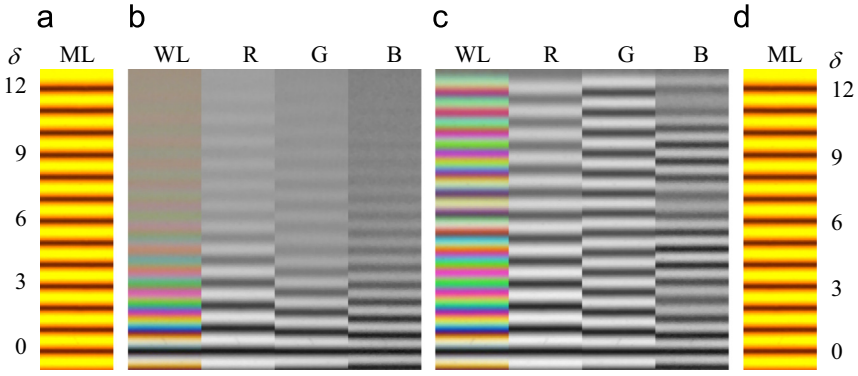

Fig. 5. Experimental isochromatic fringes in dark-field: acquired in monochromatic light (a),(d); acquired in white light shown together with the corresponding *R*, *G* and *B* signals: incandescent lamp (b), fluorescent lamp (c). [ML=monochromatic light, WL=white light]. (For interpretation of the references to color in this figure, the reader is referred to the web version of this article.)

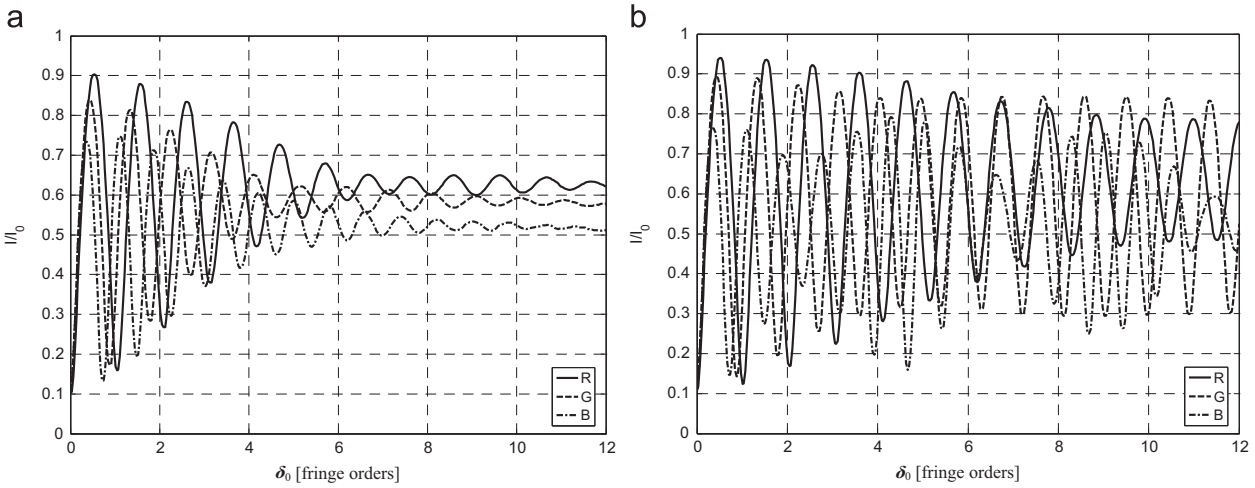

Fig. 6. Signals *R*, *G*, *B* using incandescent lamps (a) and fluorescent lamps (b) as a function of the retardation δ_0 at the reference wavelength $\lambda_0=589$ nm.

can occur using RGB photoelasticity, which is based on the analysis of colours.

Among the various methods proposed to reduce the error, the following ones have been proposed:

- Test Fringes RGB Method (TF-RGB) [74];
- Automated Tint Plate Method (ATPM) [65].

In particular, in the Test Fringes RGB Method, a Babinet compensator is inserted in series to the model to be analyzed. Thus, a system of reference fringes (isochromatics) parallel and equidistant is produced. In the Automated Tint Plate Method, a full-wave plate (usually called tint plate) is inserted in series with the model, to introduce a constant retardation, which is added algebraically with the retardation in the specimen.

In both methods, the additional device produces an increase of retardation in the zones near the fringe of order 0, where the retardation is too low to be detected with accuracy by the methods in white light. For more details on the two methods mentioned above see Section 7.2.

5.4. Methods for search of retardation

In the application of the procedure for the search of the retardation, ambiguities may occur because very similar colours (the same colours in some cases) appear for fringe orders in different ranges, starting from a certain level of the retardation itself, as it can be observed in Fig. 5. It is easy to observe that the number of similar colours at different values of the retardation increases with the increasing of δ_{max}.

This condition can be also noticed observing the three-dimensional diagram of the R, G, B levels of Fig. 7; the line representing the colours is wound as a skein (inward) with increasing retardation, as noted in [59].

Therefore, appropriate strategies to eliminate these ambiguities should be used. In general, the retardation to be determined is that for which a certain error function of the kind $e=f(R_i, G_i, B_i, R, G, B)$ is minimized, being R_i, G_i, B_i the signals stored in the calibration array and R, G, B, the signals acquired at the point of the specimen in which the retardation has to be determined.

In addition to the classic method based on the simple error function (6), the following are cited:

1. the simple error function with the subsequent imposition of the condition of continuity [43];
2. the use of the chromatic coordinates r, g, b given by (9–11) into Eq. (6), in place of the R, G and B levels [43,46,59];
3. the use of error functions that incorporate the condition of continuity [59,75];
4. the use of an error function that employs the parameters H (Hue), R-G, G-B, R-B [71];
5. the application of the median filter on the isochromatic acquired in dark field, in order to eliminate the discontinuities of the fringe order function [76];
6. the use of the classical error function evaluated over a subset of the LUT (procedure which implicitly contains the condition of continuity) [59,60,77];

Among the proposed methods, those ones based on the condition of continuity of the retardation appear to be the most effective. Table 2 shows the error functions that use the condition of continuity of the retardation in addition to the classical expression (6), renumbered as (12).

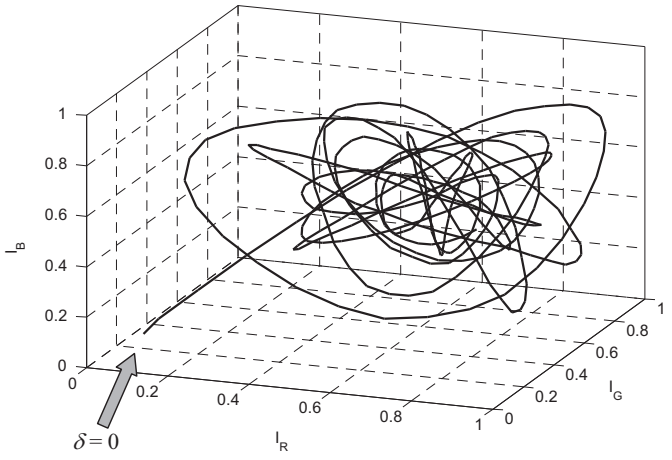

Fig. 7. I_R, I_G, I_B intensities for increasing of the retardation (taken from the experimental data of Fig. 6b).

In order to eliminate the ambiguity due to the presence of similar colours, the procedure based on (12′), that employs the condition of continuity of the unknown retardation δ with the retardation in the neighbouring pixels δ_s, was used [43].

For this purpose, applying Eq. (12′), for each pixel analyzed, in addition to the retardation δ_1, relating to the minimum error e_1 (the so-called *first result*), further retardations δ_i (i-th results) relating to errors e_i higher than e_1, are stored. Then, starting from a pixel in which the retardation was correctly determined, the actual retardation for each pixel is determined, according to the condition of continuity, that is, choosing between the values δ_i, the closest to the retardation in the previous pixel.

The error function (13) [59] and (14) [75] incorporate the condition of continuity of the unknown retardation. These relationships eliminate the ambiguity due to the similarity of colours.

The first three terms of (13) and (14), corresponding to (12) of the classical search procedure, takes into account the similarity of colours and can be defined *fidelity term*. The last term $\beta\sum_s(\delta_i-\delta_s)^2 m_s$ or $(\delta_i-\delta_s)^2K^2$ takes into account the condition of continuity of the retardation and can be defined *regularization term* or *continuity term*. The relation (13′) uses the relationship (13) applying only a part of the calibration table [59].

The error function (12″) is based on the classical error function (12) evaluated in a subset of the LUT. In the relationship (12″), i_{δ_s} is the index of the LUT corresponding to the correct value of the retardation in the pixels adjacent to the one under consideration, and Δi is given by [60]:

$$\Delta i = 0.4\,\frac{N}{\delta_N} \tag{15}$$

where N/δ_N is the number of elements of the LUT corresponding to one fringe order. The error function (12″) implicitly contains the condition of continuity of the retardation, however, it does not require the choice of parameters as required by (13) and (14) and is considerably faster than the other ones, also because it does not require any successive redetermination of the retardation.

Some refinements of this technique are described in [77]. Other comparison of the error functions, previously described, are shown in Ref [60] and [61].

In [77] the method proposed in [60] has been slightly modified in order to be applicable also for a *merged* calibration table, that is obtained by combining three different calibration tables corresponding to three different fringe gradients (determined by using the same calibration specimen under different loading conditions). In particular an interval of retardation values N_p=0.4 is used instead the interval of indexes of the LUT.

5.5. Scanning procedures

The determination of the retardation in a point (pixel) of the model by Eq. (13,13′,14,12″) requires the knowledge of the retardation in one or more pixels that are located in its neighbours. The pixels in which the retardation has been determined are defined as *resolved* or

Table 2
Types of error function used for the determination of the retardation δ.

Error function		Eq.
$e_i=\sqrt{(R-R_i)^2+(G-G_i)^2+(B-B_i)^2}$	$(0\le i\le N)$	(12)
$e_i=\sqrt{(R-R_i)^2+(G-G_i)^2+(B-B_i)^2}$ coupled in sequence with the condition of continuity of retardation	$(0\le i\le N)$	(12′)
$e_i=\sqrt{(R-R_i)^2+(G-G_i)^2+(B-B_i)^2+\beta\sum_s(\delta_s-\delta_i)^2 m_s}$	$(0\le i\le N)$	(13)
$e_i=\sqrt{(R-R_i)^2+(G-G_i)^2+(B-B_i)^2+\beta\sum_s(\delta_s-\delta_i)^2 m_s}$	$(i_{d_s}-\Delta i)\le i\le(i_{d_s}+\Delta i)$	(13′)
$e_i=\sqrt{(R-R_i)^2+(G-G_i)^2+(B-B_i)^2+K^2(\delta_s-\delta_i)^2}$	$(0\le i\le N)$	(14)
$e_i=\sqrt{(R-R_i)^2+(G-G_i)^2+(B-B_i)^2}$	$(i_{d_s}-\Delta i)\le i\le(i_{d_s}+\Delta i)$	(12″)

processed pixels, while the pixel in which the retardation has to be determined is defined as *resolving* or *processing* pixel. The procedure of determination of the retardation in a region or in all the pixels of the model is defined as *scanning* or *refining* procedure.

The principal issues of the scanning procedure are:

- the choice of the first point to be processed, also defined as *seed point* or *primary seed point*;
- the direction of scanning, that is related to the choice of the position of the resolving pixel with respect to the resolved ones;
- the selection of the resolved pixels placed in the neighbour of the resolving pixel whose δ_i or $i_{\delta s}$ parameter have to be used in Eq. (13,13′,14,12″).

Concerning the choice of the seed point, it has to be observed that usually the retardation map obtained simply using Eq. (12) presents some zones of discontinuity, but also large zones where the retardation has been correctly evaluated [43,60,77]. According to this fact, a first way to choice the seed point consists in performing a simple analysis using Eq. (12), determining a full field map of the retardation, then the operator, basing on its experience, selects a pixel inside one of these zones; the corresponding δ_i or $i_{\delta s}$ parameter is used for starting the scanning procedure [60,77]. In [59] the seed point is chosen as the one with minimum value of the sum of the RGB values that corresponds to the point with lower retardation. In [60] other two ways to choice the seed point have been proposed. In the first one, similar to that proposed in [59], the pixels belonging to the zeroth order fringes are automatically determined searching for the pixels corresponding to the minimum value of the sum of RGB values, then the operator selects one of them and the value of the δ_i or $i_{\delta s}$ parameter is set to 0. The other possibility consists of acquiring an image of the isochromatics in dark field using monochromatic light, attributing the correct (integer) fringe order to a selected dark fringe and choosing a pixel in the centre of the selected fringe (as in the centre fringe method); the value of δ_i or $i_{\delta s}$ that coincides with the integer fringe order of the selected fringe, is then introduced by the operator.

Concerning the scanning procedure, in [75] the scanning is firstly carried out for a horizontal or a vertical line starting from the primary seed point. This gives horizontal or vertical points that are refined and can be used as seed points for the scanning in orthogonal direction (*secondary* seed points). The process is called horizontal seeding or vertical seeding, accordingly.

In [60] the scanning is carried out in a way similar to that of reference [75]. The main difference consists in the fact that for the pixels of the first row and the first column, $i_{\delta s}$ is the LUT index of the previous resolved pixel, while in the other cases, it is obtained as the average LUT index of the two neighbouring pixels placed in the previous row and in the previous column (resolved pixels).

In the application of the error functions (13) and (13′) [59] all the resolved pixels surrounding the refining ones are used; in fact s denotes locations belonging to a defined neighbourhood of the refining pixel (for example, its eight surrounding pixels), m_s is a mask that indicates whether the location s has already been processed and δ_s is the refined retardation at location s.

In [77] a scanning method, termed as *advancing front scanning*, has been proposed. It progresses by resolving a pixel having maximum number of resolved neighbouring pixels within a 3×3 window centred on it at each step. The retardation value to be used in Eq. (14) or Eq. (12″) is obtained as the average value of all the adjacent neighbouring resolved pixels within the 3×3 window centred on it. The procedure starts from a single seed point or multiple seed points.

In [61] an analysis of the effect of *colour noise* on the determination of retardation has been proposed. Colour noise is a noise that can appear in isochromatics acquired in white light due to electronic noise from the camera, presence of fabrication marks on the specimen, presence of spots on the polarizer elements, and presence of dust or moisture on the optical elements. The analysis has shown that the scanning methods proposed in [75] and [60] are less sensitive to the effect of colour noise. In [61] a slight modification of the scanning method of [75] and the use of an improved RGB calibration is also proposed.

5.6. Other methods of search of the retardation

As an alternative to the RGB representation of colours in white light, the usage of the HSV/HSI (Hue, Saturation, Value)/(Hue, Saturation, Intensity) parameters has been proposed [78,79]. In particular, Tenzler and Muller have applied the above model to dynamic photoelasticity. Finally, as already said, Grewal at al. [71] use an error function that uses the hue H in addition to the R, G, B levels.

It was also given an interpretation of RGB photoelasticity as a variant of the phase shifting method, in which the shift due to the variation of the wavelength of light relative to the three images R, G, B is used [54]. However, in this case, the phase shifting is of the *multiplicative* type, different from the *additive* phase shifting commonly used in photoelasticity [80].

5.7. Considerations on the maximum detectable retardation

Using incandescent sources with continuous emission spectrum, the maximum detectable retardation is less than four fringe orders, due to the decrease of the modulation of the RGB signals.

Using fluorescent sources with discrete spectrum, the maximum detectable retardation is higher (at least 12 fringe orders [60]). As already noted, the fluorescent source with discrete emission spectrum represents the most appropriate choice of a white light source; while being simple and economical, it allows to detect the highest retardation. In this case, the limitations are mainly due to the following factors: gradient of the fringes (must be less than 0.1 orders/pixel), the presence of similar colours and the effectiveness of the procedure for the evaluation of the retardation [60].

It has also to be noted that the fluorescent light source with discrete emission spectrum produces better results also if the analysis is limited to the field $0 \le \delta \le 3$ fringe orders. This fact is due to the better modulation of the R, G, B signals obtained by the fluorescent sources respect to that obtained by the incandescent light sources, as it can be seen in Figs. 5 and 6.

5.8. Calibration on a different material and effect of light intensity

The calibration is usually carried out by means of a specimen of the same material as that of the model, using the same polariscope and the same camera (same settings). If the calibration is carried out on a material different from that of the model, the following factors must be taken into account:

- variation of colour;
- difference in the dispersion of birefringence.

The effect of the variation of colour between the material of the calibration specimen and that of the test and can be corrected by suitably modifying the LUT, as described in [64]. In addition to the image of the calibration specimen under loading, the procedure also employs bright field images of the calibration specimen and of the model without loading, whose RGB values are respectively indicated as R_{zc}, G_{zc}, B_{zc} and R_{ze}, G_{ze}, B_{ze} for the calibration specimen and the model. The modified values of the calibration table R_{mi}, G_{mi}, B_{mi} are related to the original values R_{ci}, G_{ci}, B_{ci} by the following

relations [64]:

$$R_{mi} = R_{ci}\frac{R_{zi}}{R_{zc}} \quad G_{mi} = G_{ci}\frac{G_{zi}}{G_{zc}} \quad B_{mi} = B_{ci}\frac{B_{zi}}{B_{zc}} \tag{16}$$

The effect of the change in colour using only the images of the calibration specimen and of the model under loading is considered in [81]. In particular, the R, G and B values in the calibration array are modified using the maximum and minimum R, G and B levels measured on the calibration specimen and the model; in particular, considering the signal R, the modified values of the calibration table are linked to the original values by the following equation [81]:

$$R_{mi} = (R_{ci} - R_{TableMin})\frac{R_{\mathrm{ImageMax}} - R_{\mathrm{ImageMin}}}{R_{TableMax} - R_{TableMin}} + R_{\mathrm{ImageMin}} \tag{17}$$

where the subscripts *Table* and *Image* refer respectively to the calibration specimen and the model.

The effect of the change in colour of the material and of the intensity of the reference light field is considered in [82], where it is shown that the method described in [81] is well suited in the presence of variation of the light intensity between calibration and measurement.

In the presence of the same material, but with variation of the light intensity, the chromatic coordinates r, g, b (9–11) may be used, as proposed in [43,46,59]. In particular, in [43] it is shown that, excluding the field of retardation $\delta < 0.5$, the use of chromatic coordinates allows to compensate variations of the light intensity of the source of the order of 30%. More generally, the use of chromatic coordinates allows the user to take into account of all the geometrical parameters with the exclusion, therefore, of those related to colours [59].

The previous methods do not take into account the dispersion of birefringence. The effect of the different dispersion of the birefringence between the material of the test and that of the calibration specimen is considered in [63].

Due to the effect of the dispersion of birefringence, the maximum retardation detectable by fluorescent lamp is reduced from 12 to six or even three fringe orders in dependence of the difference between the dispersions of birefringence of the calibration specimen and that of the model.

For retardations less than three fringe orders, the effect of the dispersion of birefringence is generally small (error less than 0.05 fringe orders), in the case of materials of the calibration specimen and of the model with *normal dispersion* [56] (i.e. in the case of photoelastic constant C_λ that decreases with the increase of λ). In the case of samples made by material with *anomalous dispersion* [56] (C_λ that increases with the increase of λ) and the calibration specimen is made by material with *normal dispersion*, the errors are higher.

In the case of glass, material by which it is difficult to realize the calibration specimen, the self-calibration procedure (see Section 7.2.1) has been proposed in [63]; by operating on the same material, it takes into account both the difference of colours and the dispersion of the birefringence.

6. Combined use of RGB method and phase shifting technique

Techniques based on the combined use of RGB photoelasticity and PSM have been developed for the following purposes:

1. to evaluate the isoclinic parameter and to eliminate the influence of the quarter wave plate errors in RGB photoelasticity [11,83];
2. to calibrate the retardation maps obtained by the PSM [16,17,84,85];
3. to eliminate the need of unwrapping and improve results of PSM [70,72] applying the procedure of search of the retardation of the RGB method to the wrapped retardations obtained by the PSM.

6.1. Evaluation of isoclinic parameter and elimination of quarter wave plate errors

In [11] the RGB method has been used in combination to the PSM with the aim to evaluate the isoclinic parameter and to eliminate the influence of the quarter wave plate errors in the determination of the retardation. In particular, four colour images are acquired by a plane dark field polariscope whose plates are rotated by the angles $\omega = 0$, 22.5, 45 and 67.5 degrees.

The light intensities of the four images can be expressed as

$$I_{k,j} = \frac{1}{2} I_j \sin^2 2(\alpha - \omega_k) \quad k = 1,2,3,4; \quad j = \mathrm{R,G,B} \tag{18}$$

I_j is the light intensity associated to the isochromatic fringes

$$I_j = \frac{1}{\lambda_{2j} - \lambda_{1j}} \int_{\lambda_{1j}}^{\lambda_{2j}} F_j(\lambda) I_0(\lambda) \sin^2(\pi\delta) \tag{19}$$

that can be obtained by Eq. (4) considering null the error of the retardation of quarter-wave plates.

In the evaluation of the isoclinic parameter, the RGB intensities of each image are summed in each pixel to reduce the effects of noise and of the interaction between isochromatics and isoclines, then the arctangent function is applied to a combination of the four intensities obtained. The procedure can be synthesized by the following relationship:

$$\alpha = \frac{1}{4}\tan^{-1}\frac{\sum_{j=R,G,B}(I_{4,j} - I_{2,j})}{\sum_{j=R,G,B}(I_{3,j} - I_{1,j})} \tag{20}$$

In Fig. 8, a comparison between the isoclinic maps obtained by the polariscope configurations used in ref. [11] in white light and monochromatic light is shown: it is easy to observe the higher influence of the isochromatics and of noise in the map obtained in monochromatic light. The isoclinic parameter is obtained in the field $-\pi/8 \le \alpha \le \pi/8$, so that an unwrapping procedure has to be applied.

The retardation is evaluated by the standard RGB method applied to the dark field isochromatics in white light, obtained by combining the four acquired images by the following relationship

$$I_j = \sqrt{(I_{4,j} - I_{2,j})^2 + (I_{3,j} - I_{1,j})^2} \quad j = R,G,B \tag{21}$$

Operating in this way the quarter wave plate error is obviously eliminated. It is important to notice that, in order to obtain better results, also the isochromatic fringes of the calibration model have to be determined by Eq. (21), using the four images acquired in the way previously described.

In [83] a method similar to that proposed in [11] has been applied to the case of birefringent coatings.

6.2. Calibration of the retardation maps obtained by the PSM

In [16,85] the RGB method has been used in combination with the PSM to identify the absolute value of the isochromatic parameter at a point, needed to calibrate the maps of relative retardation obtained by the PSM.

In both cases the PSM has been applied to the R, G and B levels of images acquired in white light. As it is obvious, the relationship between the retardation and the R, G and B levels of the colour images acquired by the various configurations of the polariscope

is not simply sinusoidal like Eq. (1), but similar to that shown in Eqs. (4) or (19). Nevertheless it has to be noticed that a linear relationship between the retardation and the phase values obtained by applying the arctangent functions to the intensity levels of the *R*, *G* and *B* components can be obtained [16,18,70,72], depending on the spectral properties of the filters of the camera and of the light source. In the case of the system used in ref.[16] only the green channel proved to be suitable to evaluate the retardation, while in the case of ref.[18,72] all the RGB channels were suitable, as shown in Fig. 9. It has to be noticed that the retardation obtained by phase shifting techniques applied to RGB images is not related to a specific wavelength, as it happens when a monochromatic light source is used. Therefore a reference wavelength equivalent to the combined effect of both the spectral content of the light source and the spectral response of the camera filters has to be properly selected, by a calibration of the system [18,72].

In [16] a set of six images, the first two corresponding to conventional light and dark field circular polariscope, is acquired in white light. The maps of the isoclinic parameter and of the retardation are obtained by applying the arctangent functions to a combination of the intensity levels of the green component (G) of each image; the total fringe order at a point in the fringe field, needed to carry out the unwrapping procedure, is obtained by the RGB method using the first two images.

In [85] the integration of RGB photoelasticity with phase stepping has been used to achieve automatic analysis of photoelastic fringe patterns containing a maximum fringe order not greater than four, and without the requirement for a zero-order fringe order to be present in the pattern. The PSM described is based on the acquisition of four images in white light.

6.3. Application of RGB search procedure to the retardation values obtained by the PSM instead of RGB intensities

In [70,72] the procedure of search of the retardation of the RGB method has been applied to the three maps of wrapped retardations obtained by the PSM applied to RGB images acquired by colour digital systems, rather than usual RGB intensities.

The use of the retardation values obtained by the PSM have two advantages with respect to that of the RGB intensities:

1) the influence of the spatial fluctuations of the intensity of the light source $I_0(\lambda)$ and the effect of the chromatic properties of the photoelastic material are eliminated by the PSM equations;
2) the retardation values obtained by the PSM have a better modulation, so are less prone to ambiguities when the data base search procedure is used. This second feature can be easily noticed observing Fig. 10, in which it is shown a comparison between the RGB colours obtained by a fluorescent lamp and the wrapped retardations represented as colours, obtained by properly scaling the values of retardation from the $-0.5 \le \delta \le 0.5$ field to the $0 \le R,G,B \le 255$ field.

In [70] the RGB method has been used in combination with the PSM to avoid the need for unwrapping procedure and calibration for specific materials. The polariscope configuration consists of rotating polariser and first-quarter wave plate, with the second quarter wave plate and analyser configured as a circular polariscope. The set of images for the application of the PSM are acquired in white light and three maps of wrapped retardations are obtained by applying the arctangent functions to the three combinations obtained by the R, G and B intensities of the various images. In order to improve precision, several images are acquired and a multiple regression process is employed. The determination of the retardation is carried out by the RGB photoelasticity algorithm (slightly modified) applied on the three wrapped retardations rather than on the R, G and B intensities as in the original RGB method. The values in the phase maps are properly scaled to become the R, G and B levels of a colour image. A calibration of the system has to be performed to determinate the look-up table, while it is not necessary to re-calibrate the system for different materials for the reason previously mentioned. The authors suggested to not exceed six fringe orders to avoid ambiguities in the application of the RGB algorithm.

In [72] an hybrid method has been developed with the aim to eliminate the need of the unwrapping procedure, to increase the maximum detectable fringe order of the RGB method and to reduce the effect of the isochromatics in the evaluation of the

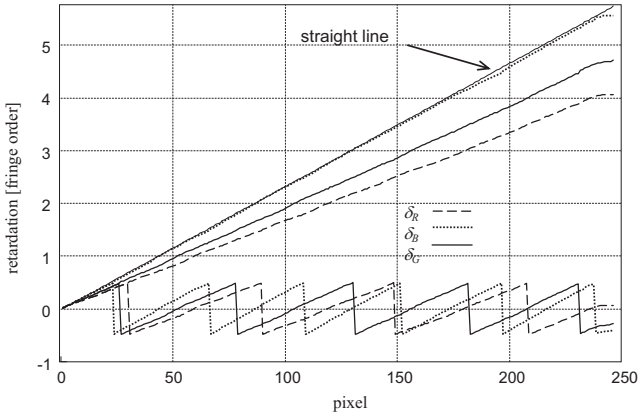

Fig. 9. Wrapped and unwrapped retardations obtained by the PSM in white light in ref. [72] in the case of a bending specimen.

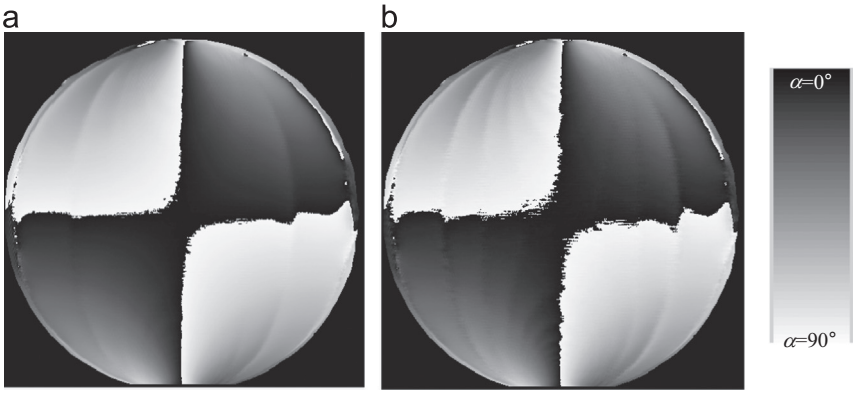

Fig. 8. Comparison between the maps of the isoclinic parameter obtained by the polariscope configuration used in ref. [11] in white light (a) and in monochromatic light (b).

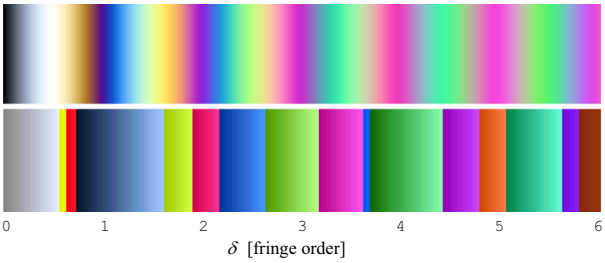

Fig. 10. Comparison between RGB colours obtained by a fluorescent lamp and the wrapped retardation represented as colours (For interpretation of the references to color in this figure, the reader is referred to the web version of this article.)

isoclinic parameter, that is carried out in a way similar to that of ref.[11]. The procedure for the determination of the retardation is similar to that of ref. [43], with the main difference that the RGB photoelasticity algorithm is used to determine only the integer part of the retardation; the fractional part is evaluated by properly averaging the values of the three phase maps obtained by the PSM equation (in this case a linear relation between the phase values and the retardation was observed). The average operation and the use of the phase values permits to minimize the effect of random errors due to noise and that introduced by various effects in the application of the RGB algorithm.

7. RGB applications

7.1. Birefringent coatings

The application of the RGB photoelasticity to the birefringent coating technique is reported in [83,86,87].

Barone and Petrucci [86] have considered the irregularity of the reflected light field as the most important problem in the application of the classical RGB method to the birefringent coatings.

The fluctuation of the light field can happen due to irregular reflectivity of the bonding surface, variations of the light incidence and reflection angles, non-uniformity of the light source. Barone and Petrucci observed that for light fluctuations less than 10%, the classic error function (6) is applicable, while for higher fluctuations the authors propose the application of the chromatic coordinate r, g and b from Eq. (9–11). In order to reduce the localised fluctuations they also recommended the application of median filtering techniques to the R, G and B values (separately), in particular in the creation of the look-up table, as described in Section 2.1.

Chang et al. [87] proposed a rather complex version of the RGB method applied to the birefringent coatings.

The LUT is build using a three point bending specimen (instead of those shown in Fig. 2) and measuring the retardation by a compensator; in particular, in the example reported, the LUT is build for retardations in the field $0 \leq \delta \leq 3$ fringe orders, with steps of 0.25 fringe orders.

The determination of the retardation in the model is carried out by the following steps:

1) a value of retardation in the LUT is chosen and a digital image containing in each pixel the corresponding RGB intensities in the LUT is created;
2) the RGB intensities of the new image are subtracted to those of the image of the model to be analyzed, generating a *difference* image;
3) the pixels of the model in which the retardation chosen in the LUT is present are selected as those in which the minimum values of the difference image are determined; in order to enhance precision, these pixels are determined binaryzing the difference image using a properly selected threshold and applying a skeleton technique.

In the article, it is not specified if the difference image is obtained by simply subtracting the two images or by applying Eq. (6). Due to the complexity of the procedure, it seems to be useful in cases in which it is not possible to realize the calibration specimen and the calibration procedure proposed in the article is performed directly on the model to be analysed, as a form of self-calibration.

Kasimayan and Ramesh [83] proposed the combined use of PSM and RGB method to evaluate both isoclinic parameter and retardation. In particular the same four images of the method proposed in [11] are acquired by the plane polariscope, while the dark field isochromatics are acquired by the circular polariscope rather than using Eq. (21).

The isoclinic parameter is evaluated by Eq. (20). The isoclinic value is unwrapped in the range $-\pi/2$ to $+\pi/2$ using the adaptive quality-guided phase unwrapping algorithm described in [88].

The retardation is determined by the RGB method using Eq. (14), that includes the condition of continuity of the retardation, and a calibration procedure that considers the differences between the colours in the measure sample and the calibration sample [64]. The total fringe order obtained is smoothed using an algorithm described in [88] to improve results. The technique is applied to various cases of industrial interest.

7.2. Residual stresses in glasses

Photoelasticity is a widely used technique for the determination of the residual stresses in glasses [89,90]. Applications of the RGB method to the membranal residual stresses on glass plates are cited by Lavrador et al. [91], while this application have been recently developed by Ajovalasit et al. [63,65,74,92].

Specifically, the following application should be cited:

- classic RGB photoelasticity by self-calibration procedure [63];
- RGB photoelasticity by means of the test fringes method (TF-RGB: *Test fringes* RGB Method) [74];
- RGB photoelasticity by means the use of a Tint Plate (ATPM: Automated Tint Plate Method) [65].

By means of opportune precautions, the cited techniques could be applied to the analysis of the residual strains of polymeric material [93,94].

In the next sections, the three methods mentioned above are briefly described.

In addition, a method for the residual stress analysis of glasses based on the analysis of the RGB colours is described in ref. [95].

7.2.1. Classic RGB photoelasticity

The RGB Method can be directly applied to the membrane residual stress analysis of glass plates. Due to the difficult manufacture of a calibration specimen of the same material of the model to analyse, a specific calibration procedure has to be adopted, the so called *self-calibration* [63]. The self-calibration procedure consists on the creation of the LUT by using the colour levels acquired in the same glass plate of the model to analyse (or in a different plate of the same material). The retardation needed for the calibration has to be determined by a different method as the phase shifting method. In this way, it is not necessary to make the calibration between two integer fringes, but the only one condition to absolve is that the selected section for the calibration should to have the maximum retardation δ_{0N} not lesser than the ones to acquire in the model.

Due to the probable non-linearity of the retardation in the calibration section, the LUT created by simply storing the acquired intensity triplets and the correspondence retardation δ_{0i} presents a non-linear relationship between these stored values and the indexes i, than this *correspondence* LUT cannot be directly applied for the determination of the retardation with the Eq. (5). A linearization procedure has to be applied to obtain a *linearized* LUT by means an opportune interpolation procedure described in [63].

As an examples, in Fig. 11(a) the window glass of a car, in the zone near a hole, is shown. The calibration has been made in a section near a corner of the same glass shown in Fig. 11(b). As it is possible to note by the colour of the figures, the retardation of the calibration section is bigger than the one in the image to analyse.

7.2.2. TF-RGB, Test Fringes RGB Method

In this technique, a Babinet sample or a simple bended beam, here called Carrier, is superimposed to the sample to analyse, as shown in Fig. 12. The Babinet sample introduce a system of parallel and equidistant fringes. This fringe system, usually called *test fringes* [89], effectively reveal the presence of residual stresses.

As an example, Fig. 13 shows the fringe system in the carrier lonely (top part of the image) and in the glass superimposed to the carrier (bottom part of the image).

The use of the RGB method by means of a fringe system in monochromatic light is reported in [74] and re-treated in [96] and [97].

7.2.3. ATPM, The Automated Tint-Plate Method

The automatic analysis, based on the use of the tint plate, was proposed by Ivanova and Nechev [98] and by Sanford and McGinnis [99] in conjunction with the SCA method (Spectral Content Analysis). The use of RGB photoelasticity jointly to the tint plate, initially proposed in a qualitative way [91], has been further developed in [65].

The technique consists in inserting in series with the glass specimen a full-wave plate, usually called tint plate, with the optical axes aligned with the directions of the glass principal stresses. The tint plate introduces a constant retardation, which is added algebraically with the retardation in the glass. As shown in Fig. 14, the isochromatic fringes visible in absence (a) and in presence (b) of the Tint Plate are different.

The polariscope is the same as that shown in Fig. 12 where the tint plate is inserted in place of the carrier C. The use of the tint plate is particularly useful near the fringe of zeroth order where the retardation is low and significant measurement errors can be achieved when RGB photoelasticity is used, as it is well known.

Fig. 15 shows the direct comparison between the ATPM, the RGB method and the TF-RGB method in the zone of the measurement section with retardation not higher than half fringe order. The retardation evaluated by the TMCM and the principal stress difference are also shown. The analysis of Fig. 15 clearly shows the benefit of using the tint plate (ATPM) or the reference fringes (TF-RGB) in the presence of fringe orders lower than 0.5 fringe orders.

7.2.4. Other applications

As other applications, the following are reported:

1) SIF determination in thermal stressed disks [100], in bi-material joints [101–103] and in plate with periodical distribution of blind holes [62];
2) the effect of defence holes for the decrease of stress concentration in perforated plates [104,105];
3) developing of full field sensors [106];

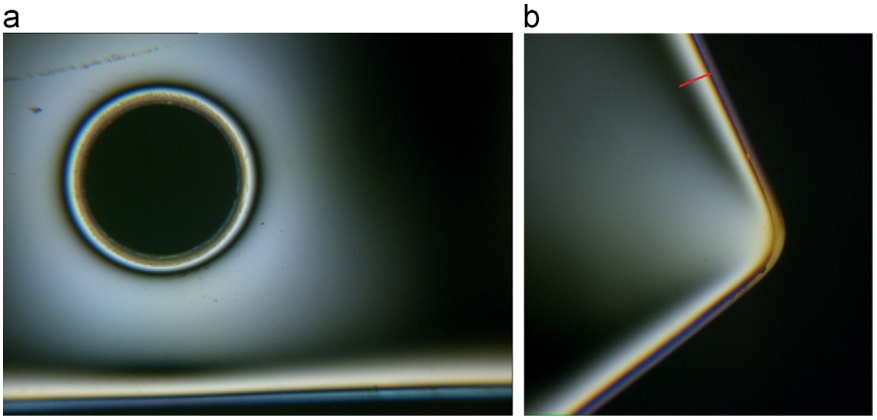

Fig. 11. Dark filed circular polariscope image in white light of a car window glass near a hole (a) and section selected (-) for the self-calibration procedure of the RGB method (b). (For interpretation of the references to color in this figure, the reader is referred to the web version of this article.)

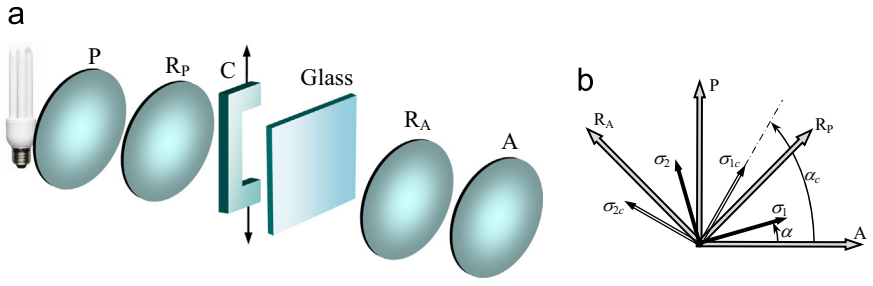

Fig. 12. Test fringes method: (a) polariscope, (b) orientation of the optical elements. (C: carrier, P,A: polarizers, R_p,R_a: quarter wave plates, σ_1,σ_2: glass principal stresses, σ_{1c}, σ_{2c}: carrier principal stresses, α,α_c: orientation of principal stresses respectively in the glass and in the carrier).

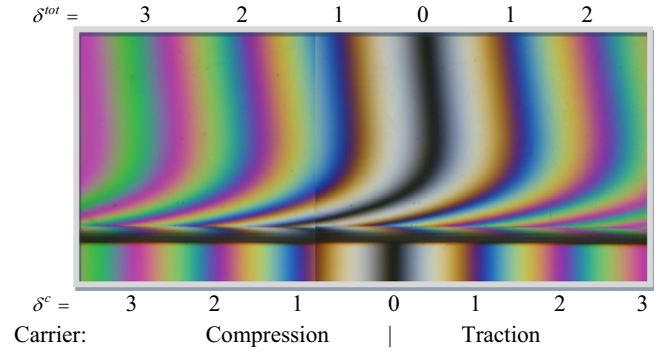

Fig. 13. Isochromatic fringes (colour figure in the online version of the article) using white light and a dark circular polariscope: in the carrier (bottom part) and in the glass superimposed to the carrier (top part) (For interpretation of the references to color in this figure, the reader is referred to the web version of this article.)

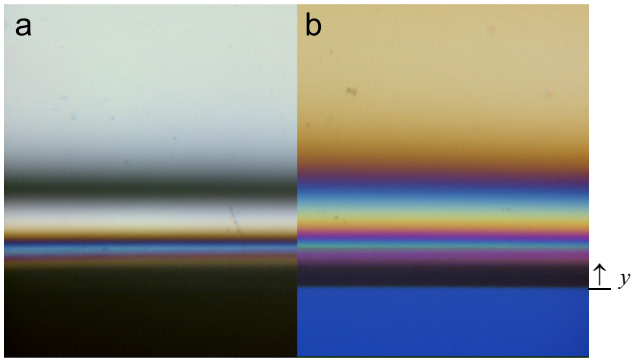

Fig. 14. Isochromatic in absence (a) and in presence (b) (For interpretation of the references to color in this figure, the reader is referred to the web version of this article.)

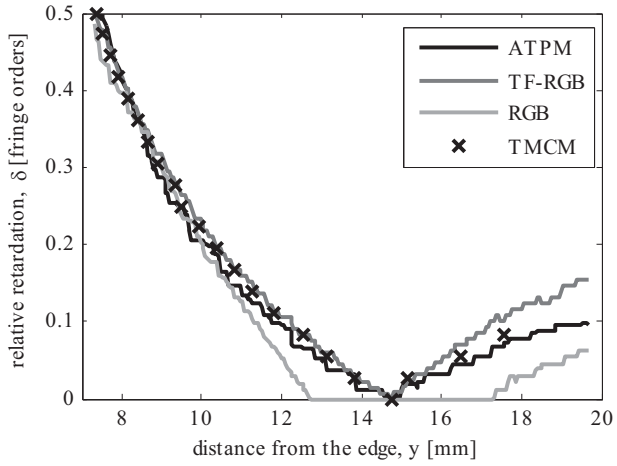

Fig. 15. Comparison between the ATPM, the TF-RGB method, the RGB method and the TMCM for low retardations ($\delta \leq 0.5$ fringe orders).

4) fringe order determination in "slices" derived by a 3D sample made by stereo-lithography [107] where is shown that PSM and RGB photoelasticity give equivalent results;
5) the application of RGB techniques to the analysis of the deformation in polymeric films [108,109].

Other additional applications are reported in reference [4].

8. Conclusions

In this article, a review of the RGB photoelasticity is presented. The peculiarities of this technique consist in the fact that the images are acquired in white light by a colour digital image processing system and the retardation is determined by a data base search approach. RGB photoelasticity allows the users to determine the photoelastic relative retardation by means of a single image, without the need of external information, although a calibration procedure has usually to be performed.

The use of four images acquired by a plane dark field polariscope allows to determinate the isoclinic parameter minimising the influence of the isochromatics and eliminating the errors due to the quarter wave plates.

The combined use of RGB photoelasticity and PSM can be considered in the presence of high fluctuations of the reference light field or to eliminate the need to perform calibration for the various materials or in the need of higher precision.

The highest retardation detectable by this technique has grown from three-four fringe orders of the first applications, to twelve (at least) fringe orders, thanks principally to the use of discrete spectrum light sources and the application of refined retardation research procedures.

In particular, various commercially available fluorescent lamps allows us to determine retardations up to 12 fringe orders, owing to the discrete nature of the source that is approximately equivalent to three sources with a narrow band spectrum approximately centred in the wavelengths fields of the *R*, *G* and *B* colours. In such a case, the limitation of the maximum fringe order derives mainly from the gradient of the fringes, from the presence of similar colours and from the effectiveness of the procedure of search of the retardation. The fluorescent lamp can be considered as the best low-cost solution; however, it is worth noting the proposal to use good quality RGB LED as source for RGB photoelasticity. In order to maximize the modulation of the RGB signals acquired, some care in the regulations of the digitizing hardware must be adopted, in particular as regards the aperture of the lens of the camera and the white balance adjustment of the acquisition system.

The procedures of determination of the retardation based on the use of a continuity condition are very effective. In particular, the one that determine the retardation by means of a limited LUT implicitly contains the condition of continuity of the retardation. Unlike procedures that explicitly contain the condition of continuity, it does not require the choosing of any parameter and it results considerably faster than the other ones.

The calibration procedure is usually made by a sample of the same material of the measurement specimen. If the calibration is made using a sample made of a different material it is important to take into account the colour variation and the birefringence dispersion. For retardation lower than three fringe orders, the effect of the dispersion of the birefringence is usually negligible (with the condition that the measurement and the calibration sample have the same type of birefringence dispersion). In some cases it may be useful to employ a self-calibration procedure.

In determination of the LUT by using a bending specimen, it is recommended that each *R*, *G* and *B* level is determined as the median of the values acquired along a line parallel to the fringes. The most advantageous shape of the calibration bending specimen is that represented in Fig. 2a, while, if the maximum easy of construction is necessary, the four points bending specimen or the eccentrically loaded tensile specimen used by some authors can be considered.

RGB photoelasticity can be considered as one of the most important techniques for the automation of the photoelastic method, so that it can find useful application in different field of

experimental stress analysis, such as the analysis of residual stresses in birefringent materials as glass and polymers, commonly used in various products.

The analysis of residual stresses in the glass is definitely an important example of the application of the RGB photoelasticity.

References

[1] Ajovalasit A, Barone S, Petrucci G. A review of automated methods for the collection and analysis of photoelastic data. J Strain Anal 1998;**33**:75–91.
[2] Ramesh K, Mangal SK. Data acquisition techniques in digital photoelasticity: a review. Opt Lasers Eng 1998;**30**:53–75.
[3] Patterson EA. Digital photoelasticity: principles, practice and potential. Strain 2002;**38**:27–39.
[4] Ramesh K, Kasimayan T, Neethi Simon B. Digital photoelasticity–A comprehensive review. J Strain Anal 2011;**46**:245–66.
[5] Solaguren-Beascoa Fernandz M. Data acquisition techniques in photoelasticity. Exp Tech 2011;**35**(6):71–9.
[6] Hecker FW, Morche B. Computer-aided measurement of relative retardations in plane photoelasticity. In: Wieringa H, editor. Experimental stress analysis. Leiden, Nederland: Martinus Nijhoff Publishers; 1986. p. 535–42.
[7] Patterson EA, Wang ZF. Towards full field automated photoelastic analysis of complex components. Strain 1991;**27**(2):49–56.
[8] Ajovalasit A, Barone S, Petrucci G. A method for reducing the influence of quarter-wave plate errors in phase stepping photoelasticity. J Strain Anal 1998;**33**(3):207–15.
[9] Barone S, Burriesci G, Petrucci G. Computer aided photoelasticity by an optimum phase stepping method. Exp Mech 2002;**42**(2):132–9.
[10] Ramesh K. Photoelasticity. In: Sharpe, editor. in springer handbook of experimental solid mechanics. Berlin: Springer; 2008.
[11] Petrucci G. Full field evaluation of an isoclinic parameter in white light. Exp Mech 1997;**37**(4):420–6.
[12] Zhenkun L, Dazhen Y, Wanming Y. Whole-field determination of isoclinic parameter by five-step colour phase shifting and its error analysis. Opt Lasers Eng 2003;**40**(3):189–200.
[13] Pinit P, Umezaki E. Digitally whole-field analysis of isoclinic parameter in photoelasticity by four-step colour phase-shifting technique. Opt Lasers Eng 2007;**45**(7):795–807.
[14] Kihara T. Automatic whole-field measurement of principal stress directions using three wavelengths. Proceedings of the tenth international conference on experimental mechanics 1994;1:95–9 (Lisbon).
[15] Ji W, Patterson EA. Simulation of errors in automated photoelasticity. Exp Mech 1998;**38**(2):132–9.
[16] Ramesh K, Deshmukh SS. Automation of white light photoelasticity by phase-shifting technique using colour image processing hardware. Opt Lasers Eng 1997;**28**(10):47–60.
[17] Ramesh K, Mangal SK. Automation of data acquisition in reflection photoelasticity by phase shifting methodology. Strain 1997;**33**:95–100.
[18] Ajovalasit A, Petrucci G, Scafidi M. Phase shifting photoelasticity in white light. Opt Lasers Eng 2007;**45**(5):596–611.
[19] Quan C, Bryanstone-Cross PJ, Judge TR. Photoelasticity stress analysis using carrier fringe and FFT techniques. Opt Lasers Eng 1993;**18**(2):79–108.
[20] Ajovalasit A, Zuccarello B. Limitation of Fourier transform photoelasticity: influence of isoclinics. Exp Mech 2000;**40**(4):384–92.
[21] Ajovalasit A, Pitarresi G, Zuccarello B. Limitation on carrier fringe methods in digital photoelasticity. Opt Lasers Eng 2007;**45**(5):631–6.
[22] Zuccarello B, Tripoli G. Photoelastic stress pattern analysis using Fourier transform with carrier fringes: influence of quarter-wave plate error. Opt Lasers Eng 2002;**37**:401–16.
[23] Sanford RJ. On the range of accuracy of spectrally scanned white light photoelasticity. Proceeding of the SEM conference on experimental mechanics 1986:901–8 (New Orleans).
[24] Sanford RJ, Iyengar V. The measurement of the complete photoelastic fringe order using a spectral scanner. Proceeding of the SEM conference on experimental mechanics 1985:160–8 (Las Vegas).
[25] Voloshin AS, Redner AS. Automated measurement of birefringence: development and experimental evaluation of the techniques. Exp Mech 1989;**29**(3):252–7.
[26] Haake SJ, Patterson EA. Photoelastic analysis using a full field spectral contents analyser. Proceeding of the SEM conference on experimental mechanics 1995:342–5 (Gran Rapids, Michigan).
[27] Lesniak JR, Zickel MJ, Welch CS, Johnson DF. An innovative polariscope for photoelastic stress analysis. Proc. Soc. For Exp. Mech., Spring Conference 1997 (June).
[28] Yoneyama S, Gotoh J, Takashi M. Tricolour photoviscoelastic technique and its application to moving contact. Exp Mech 1998;**38**(3):211–7.
[29] Yoneyama S, Shimizu M, Gotoh J, Takashi M. Photoelastic analysis with a single tricolour image. Opt Lasers Eng 1998;**29**:423–35.
[30] Ekman MJ, Nurse AD. Absolute determination of the isochromatic parameter by load-stepping photoelasticity. Exp Mech 1998;**38**(3):189–95.
[31] Ramesh K, Tamrakar DK. Improve determination of retardation in digital photoelasticity by load stepping. Opt Lasers Eng 2000;**33**:387–400.
[32] Liu T, Asundi A, Boay CG. Full field automated photoelasticity using two-load-step method. Opt. Eng. 2001;**40**(8):1629–35.
[33] Nurse AD. Load-stepping photoelasticity: new developments using temporal phase unwrapping. Opt Lasers Eng 2002;**38**:57–70.
[34] Ramesh K, Pathak PM. Role of photoelasticity in evolving discretization schemes for FE analysis. Exp Tech 1999;**23**(4):36–8.
[35] Ragulskis, M., Ragulskis, L. Plotting isoclinics for hybrid photoelasticity and finite element analysis. *Experimental mechanics*. **44**(3), 235-240.
[36] Ragulskis M, Ragulskis L. On interpretation of fringe patterns produced by time average photoelasticity. Exp Tech 2005;**29**(3):48–51.
[37] Wang WC, Tsai YH. Time-averaged photoelastic stress analysis of the ultrasonic wave in a strip. Exp Mech 2006;**46**(6):757–63.
[38] Umezaki E, Nanka Y, Shimamoto A. Assignment of fringe orders to RGB Photoelastic fringes. International Cong. on advanced technology in experimental mechanics 1999:87–92 (ATEM '99).
[39] Umezaki E, Kodama K, Shimamoto A. Evaluating the stress intensity factor using white light photoelastic experiment. Metal Mater Int 2001;**7**(1):49–53.
[40] Kodama K, Umezaki E. Extraction and Multiplication of isochromatics using linearly polarized RGB lights. APCFS & ATEM '01, JSME-MMD 2001:766–71 (JSME N° 01-203).
[41] Quiroga JA, Servin M, Marroquin JL. Regularized phase tracking technique for demodulation of isochromatics from a single tricolour image. Meas Sci Technol 2002;**13**:132–40.
[42] Ajovalasit A, Petrucci G. Analisi automatica delle frange fotoelastiche in luce bianca. Proceedings of the XVIII AIAS conference 1990:395–407 (Istituto di Ingegneria Meccanica, Università di Salerno).
[43] Ajovalasit A, Barone S, Petrucci G. Toward RGB photoelasticity - Full field photoelasticity in white light. Exp Mech 1995;**35**(3):193–200.
[44] Ajovalasit A, Barone S, Petrucci G. Automated photoelasticity in white light: influence of quarter-wave plates. J Strain Anal 1995;**30**(1):29–34.
[45] Ramesh K, Deshmukh SS. Three fringe photoelasticity - use of colour image processing hardware to automate ordering of isochromatics. Strain 1996;**32**(3):79–86.
[46] Yoneyama S, Takashi M. A new method for photoelastic fringe analysis form a single image using elliptically polarized white light. Opt Lasers Eng 1998;**30**:441–59.
[47] Desse JM. Three colour differential interferometry. Appl Opt 1997;**36**:7150–6.
[48] Ho H, Qin YW. Digital colour encoding and its application to the moiré technique. Appl Opt 1997;**36**:3682–5.
[49] Huang PS, Hu Q, Jin F, Chiang FP. Colour–encoded digital fringe projection technique for high-speed three-dimensional surface contouring. Opt Eng 1999;**38**(6):1065–71.
[50] Gomez-Pedrero JA, Quiroga JA, Terron-Lopez MJ, Servin M. Measurement of surface topography by RGB shadow-moirè with direct phase demodulation. Opt Lasers Eng 2006;**44**:1297–310.
[51] Montarou CC, Gaylord TK, Villalaz RA, Glytsis EN. Colourimetry-based retardation measurement method with white-light interference. Applied Optics 2002;**41**(25):5290–7.
[52] Chen, T.Y., Editor, Selected papers on photoelasticity. *SPIE milestone series*, vol. MS 158, 1999, 276-83.
[53] Chen TY. Digital photoelasticity in *photomechanics*. In: Rastogi PK, editor. Berlin: Springer; 2000. p. 221.
[54] Sciammarella CA, Sciammarella FM. Experimental mechanics of solids. Wiley; 2012.
[55] Haake SJ, Patterson EA. The dispersion of birefringence in photoelastic materials. Strain 1993;**29**(1):3–7.
[56] Cloud G. Optical methods of engineering analysis. Cambridge University Press; 1995.
[57] Yoneyama S, Shimizu M, Takashi M. Higher retardation analysis in automated white light photoelasticity. Proceedings of the eleventh international conference on experimental mechanics 1998;1:527–32 (Oxford (UK).
[58] Scalzo P, Gottardi G, Freddi A. Contributo allo studio di metodi avanzati per l'analisi digitale a campo intero delle frange isocromatiche. Proceedings of the XXVII AIAS conference 1998:1095–104 (Perugia).
[59] Quiroga JA, Garcia-Botella A, Gomez-Pedrero JA. Improved method for isochromatic demodulation by RGB calibration. Appl Opt 2002;**41**:3461–8.
[60] Ajovalasit A, Petrucci G, Scafidi M. RGB Photoelasticity: review and improvements. Strain 2010;**46**(2):137–47.
[61] Swain D, Philip J, Pillai SA. A modified regularize scheme for isochromatic demodulation in RGB photoelasticity. Opt Lasers Eng 2014;**61**:39–51.
[62] Cirello A, Furgiuele F, Maletta C, Pasta A. Numerical simulations and experimental measurements of the stress intensity factor in perforated plates. Eng Fract Mech 2008;**75**:4383–93.
[63] Ajovalasit A, Petrucci G, Scafidi M. RGB photoelasticity applied to the analysis of membrane residual stress in glass. Meas Sci Technol 2012;**23**(2) (art. n. 025601).
[64] Mandhu KR, Prasath RGR, Ramesh K. Colour adaptation in three fringe photoelasticity. Exp Mech 2007;**47**(2):271–6.
[65] Ajovalasit A., Petrucci G., Scafidi M., Photoelastic analysis of edge residual stresses in glass by the automated tint plate method. *Experimental techniques* (article in press). doi:10.1111/ext.12017.
[66] Yoneyama S, Gotoh J, Takashi M. Experimental analysis of rolling contact stresses in a viscoelastic strip. Exp Mech 2000;**40**(2):203–10.
[67] Yoneyama S, Takashi M. Elliptical polarized white light photo viscoelastic technique and its application to viscoelastic fracture. Opt Lasers Eng 2002;**38**:17–30.

[68] Ajovalasit A, Barone S, Petrucci G, Zuccarello B. The influence of the quarter wave plates in automated photoelasticity. Opt Lasers Eng 2002;**38**:31–56.
[69] Petrucci G. Un sistema completo per l'elaborazione delle frange fotoelastiche in luce bianca. Proceedings of the XX AIAS conference 1991:121–33 (Palermo).
[70] Jones IA, Wang P. Complete fringe order determination in digital photoelasticity using fringe combination matching. Strain 2003;**39**(3):121–30.
[71] Grewal GS, Dubey VN, Claremont DJ. Isochromatic demodulation by fringe scanning. Strain 2006;**42**:273–81.
[72] Ajovalasit A, Petrucci G. Developments in RGB photoelasticity. Appl Mech Mater 2005;**3-4**:205–10.
[73] Ng TW, Asundi A. Light emitting diodes for illumination in photoelasticity. Exp Tech 1997;**21**(4):28–30.
[74] Ajovalasit A, Petrucci G, Scafidi M. Photoelastic analysis of edge residual stresses in glass by automated test fringes methods. Exp Mech 2012;**52**(8):1057–66.
[75] Madhu KR, Ramesh K. Noise removal in three fringe photoelasticity by adaptive colour difference estimation. Opt Lasers Eng 2007;**45**:175–82.
[76] Dubey VN, Grewal GS. Noise removal in three-fringe photoelasticity by median filtering. Opt Lasers Eng 2010;**47**:1226–30.
[77] Kale S, Ramesh K. Advancing front scanning approach for three-fringe photoelasticity. Opt Lasers Eng 2013;**51**(5):592–9.
[78] Tenzler A, Mueller DH. Untersuchung von FVL mit Hilfe der Spannungsoptik. VDI Ber 1991;882:99–108 (n).
[79] Hoy DEP. On the use of colour imaging in experimental applications. Exp Tech 1997;**21**(4):17–9.
[80] Vargas J, Quiroga JA, Sorzano COS, Estrada JC, Servin S. Multiplicative phase-shifting interferometry using optical flow. Appl Opt 2012;**51**(24):5903–8.
[81] Neethi Simon B, Ramesh K. Colour adaptation in three fringe photoelasticity using a single image. Exp Tech 2011;**35**(5):59–65.
[82] Neethi Simon B, Kasimayan T, Ramesh K. The influence of ambient illumination on colour adaptation in three fringe photoelasticity. Opt Lasers Eng 2011;**49**:258–64.
[83] Kasimayan T, Ramesh K. Digital reflection photoelasticity using conventional reflection polariscope. Exp Tech 2010;**34**(5):45–51.
[84] Carazo-Alvarez J, Haake SJ, Patterson EA. Completely automated photoelastic fringe analysis. Opt Lasers Eng 1994;**21**:133–49.
[85] Patterson EA, Wang ZF. Integration of spectral and phase-stepping methods in photoelasticity. J Strain Anal 1999;**34**(1):59–64 (1999).
[86] Barone S, Petrucci G. Automated photoelasticity in white light: application to birefringent coatings. XIII IMEKO world conference. 1994.
[87] Chang CW, Lien HS, Lin JH. Determination of reflection photoelasticity fringes analysis with digital image-discrete processing. Measurement 2008;**41**(8):862–9.
[88] Ramji M, Ramesh K. Whole field evaluation of stress components in digital photoelasticity-issues, implementation and application. Opt Lasers Eng 2008;**46**(3):257–71.
[89] Aben H, Guillemet C. Photoelasticity of glass. Berlin: Springer – Verlag; 1993.
[90] McKenzie HW, Hand RJ. Basic Optical Stress measurement in glass. Sheffield, U.K: Society of Glass Technology; 1999.
[91] Lavrador MB, Soares ACC, Vieira RD, Freire JLF. Automated inspection of residual stresses in glass using RGB Photoelasticity. Proceedings of the 1998 SEM spring conference 1998:124–7 (Houston, 1-3 June).
[92] Ajovalasit A, Petrucci G, Scafidi M. A critical assessment of automatic photoelastic methods for the analysis of edge residual stresses in glass. J Strain Anal Eng Des 2014;**49**(5):361–75.
[93] ASTM D 4093, Standard test method for photoelastic merasurement of birifrangence and residual strains in transparent or translucent plastic materials. *Annual book of ASTM standards*.
[94] Redner AS, Nickola WE. Measurement of residual strains and stresses in transparent materials. Exp Tech 1984:29–32 (Feb).
[95] Coelho JM, Silva C, Almeida T. Stress Analysis in glass art work. Int J Opt 2011. http://dx.doi.org/10.1155/2011/215404 (Article ID 215404).
[96] Naveen YA, Ramesh K, Ramakrishnan Vivek. Use of carrier fringes in the evaluation of edge residual stresses in a glass plate by photoelasticity. Joint international conference "ISEM-ACEM-SEM-seventh ISEM'12-Taipei" 2012 (Taipei, Taiwan, paper/J106, in internet at).
[97] Ramesh K, Vivek R, Tarkes Dora P, Sanyal D. A simple approach to photoelastic calibration of glass using digital photoelasticity. J Non-Cryst Solids 2013;**378**:7–14.
[98] Ivanova L, Nechev G. A method for investigation of the residual stressed in glasses with spectral polariscope. Proceedings of the nineth international conference on experimental mechanics 1990;2:876–83 (Copenhagen).
[99] Sanford RJ, McGinnis A. New method for measuring low level birefringence using a spectra scanner. Proceedings thirty seventh international instrumentation symposium 1991:1029–41 (ISA-Instrument Society of America, San Diego, May).
[100] Barone S, Pasta A, Petrucci G. Stress intensity factors in hollow disks under thermal loading. Proceedings International Conference on Experimental Mechanics 1994:183–8 (Lisbona).
[101] Barone S, Pasta A. Photoelastic determination of stress intensity factors in biomaterial joints by using an automated technique. ICCE/2 s international conference on composites engineering 1995:51–2 (New Orleans, LA (USA).
[102] Cirello A, Zuccarello B. On the effects of a crack propagating toward the interface of a bimaterial system. Eng Fract Mech 2006;**73**(9):1264–77.
[103] Neethi Simom B, Prasath RGR, Ramesch K. Transient thermal stress intensity factors of biomaterial interface cracks using refined three-fringe photoelasticity. J Strain Anal 2009;**44**(6):427–38.
[104] Akour SN, Nayfeh JF, Nicholson DW. Design of a defence hole system for a shear-loaded plate. J Strain Anal Eng Des 2003;**38**(6):507–17.
[105] Akour SN, Nayfeh JF, Nicholson DW. Defence hole design for a shear dominant loaded plate. Int J Appl Mech 2010;**2**(2):381–98.
[106] Dubey VN, Grewal GS. Efficacy of photoelasticity in developing whole-field imaging sensors. Opt Lasers Eng 2009;**48**:288–94.
[107] Ashokan K, Prasath RGR, Ramesh K. Noise-free determination of isochromatic parameter of stereolithography–built models. Exp Tech 2012;**36**(2):70–5.
[108] Brinez JC, Giraldo FL, Martinez AR, Perfiles RGB. en analisis digital de imagenes para la description de los coloures de interferencia producidos un estudios de fotoelasticitad de la deformacion de peliculas plasticas. XVII *Simposio de Tratamiento de Senales, Imagenes Y Vision Artificial* 2012 (Stsiva).
[109] Restrepo-Martínez A, López F. Color spaces analysis of photoelasticity images of plastics thin films. Optics infobase conference 2011.